HiSST: 3rd International Conference on
High-Speed Vehicle Science Technology
14 -19 April 2024, Busan, Korea

Assessment of Thermochemical Degradation Effects of Charring Material on the Wall Heat Flux during Atmospheric Re-Entry

Maxime Lalande[1], Nicolas Dellinger[2], Ysolde Prévereaud[3], Nathalie Bartoli[4,5]

Abstract

Models providing both quick and reliable estimates of thermochemical degradation effects of charring material on the wall heat flux in hypersonic continuum flow regime are paramount for design activities. In this work, flight point conditions have been extracted from numerous complete trajectory simulations, which are representative of atmospheric re-entry from Low Earth Orbit. High-fidelity simulations are carried out on these flight points to evaluate the influence of pyrolysis gas blowing on wall heat flux modification, with particular attention paid to chemical non-equilibrium effects and outgassed species composition. Additionally, a comparison of two models used to calculate the mixture transport properties is conducted.

Keywords: *Aerothermodynamics, Gas-surface interactions, Material degradation, Atmospheric entry, CFD numerical simulation*

Nomenclature

A – Arrhenius pre-exponential constant
D – Diameter [m]
E_A – Activation energy [J/mol]
$\Delta_f H^0$ – Standard formation enthalpy [J/mol]
$\Delta_r H^0$ – Standard reaction enthalpy [J/mol]
Kn – Knudsen number
L – Length [m]
M – Mach number
Pr – Prandtl number
Sc – Schmidt number
T – Temperature [K]
V – Velocity [m/s]
d – Distance [m]
e – Thickness [m]
$\dot{m}$ – Pyrolysis gas mass flux [kg/m²/s]
p – Pressure [Pa]
z – Altitude [m]
α – Object angle of attack
γ – Object entry slope angle
ε – Material emissivity
ν – Stoichiometric coefficient
$\dot{\omega}$ – Molar production rate [mol/m³/s]
$\dot{\omega}_T$ – Total chemical heat release rate [J/m³/s]
ρ – Density [kg/m³]
ϕ – Heat flux [W/m²]

Subscripts
ab – Ablation
c+d – Convective-diffusive
cond – Conduction
stag – Stagnation point
w – Wall
0 – Reference
∞ – Freestream value

1. Introduction

The significant aerothermal heating encountered during the atmospheric re-entry is responsible for the thermochemical degradation of materials. So, the wall heat flux estima-

1 *DMPE, ONERA, Université de Toulouse, 31000, Toulouse, France, maxime.lalande@onera.fr*
2 DMPE, ONERA, Université de Toulouse, 31000, Toulouse, France, nicolas.dellinger@onera.fr
3 DMPE, ONERA, Université de Toulouse, 31000, Toulouse, France, ysolde.prevereaud@onera.fr
4 DTIS, ONERA, Université de Toulouse, 31000, Toulouse, France, nathalie.bartoli@onera.fr
5 Fédération ENAC ISAE-SUPAERO ONERA, Université de Toulouse, 31000, Toulouse, France

tion is essential for the space mission design. For hypersonic objects (vehicles, capsules, space debris, etc.) made of charring materials, pyrolysis gases are blown into the boundary layer and physico-chemical processes occur at the gas-surface interface (catalytic recombination, oxidation, nitridation, sublimation, etc.). Together, these phenomena modify the flow chemical composition, the surface geometry, and the convective-diffusive heat flux, which in turn drives the material thermochemical response. Thus, there is a strong physical coupling between the flow and the material. High-fidelity tools can be used to model these phenomena but are too costly to perform complete trajectory calculations. The correlations used in atmospheric re-entry codes enable fast modelling of vehicle aerothermodynamics but do not take into account most fluid-solid interactions. Supervised machine learning techniques based on high-fidelity simulations is expected to provide surrogate models giving a rapid and more accurate evaluation of heat flux. However, the use of these methods requires the input and output variables that characterise the phenomenon under consideration to be properly identified. Then, a suitable database can be developed and used to train and validate the model. An important step of this work is to carry out a comprehensive study of the fluid-structure physical phenomena known and to identify those playing a major role on the wall heat flux during the thermochemical degradation of charring materials. This will allow prioritizing and defining the phenomena to consider for the development of such a database.

Section 2 describes the methodology employed to define a range of wall temperature, pyrolysis gas mass blowing rate, and freestream conditions characteristic of Low Earth Orbit (LEO) re-entry. In Section 3, CFD simulations are carried out to evaluate the influence of pyrolysis gas blowing on wall heat flux modification, with particular attention paid to chemical non-equilibrium effects between air and outgassed species in the boundary layer, for different flight conditions. In Section 4, the effects of different models used to calculate the mixture transport properties on the wall heat flux are examined.

2. Complete re-entry trajectories simulation methodology

It is first necessary to define a set of characteristic flight points for spacecraft and space debris re-entering the atmosphere, on which high-fidelity simulations will be run to assess the importance of fluid-structure phenomena, and finally develop the learning database. To this end, complete reentry trajectories are simulated using the vehicle-oriented code ARES [1] on a set of four different simple hollow geometries: sphere $(D=200-1200\,mm)$, spheric-cylinder and cylinder ($L=500-2850\,mm$, $L/D=1.25-2.8$), and a fuel tank from JAXA ($L=662-1261\,mm$, $D=760-1250\,mm$) [2], see Fig. 1. These objects are composed of an external Carbon Fiber Reinforced Polymer (CFRP) composite layer of thickness $e_{CFRP}=2-15\,mm$ and an inner metal liner of $e_{Li}=1$ or $2\,mm$, which is representative of space debris such as Composite Overwrapped Pressure Vessel (COPV).

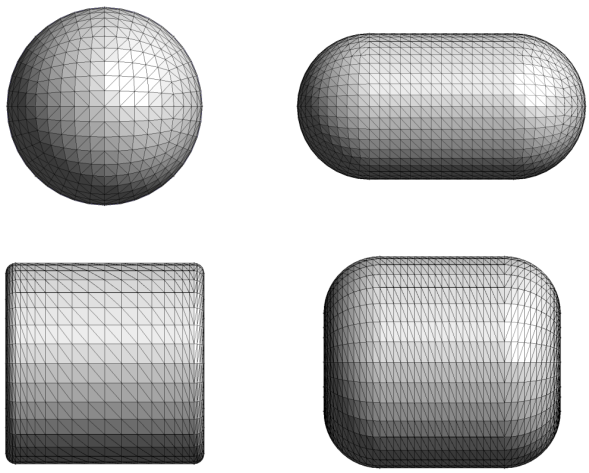

Fig 1. Geometries of considered objects.

Aerothermodynamic modelling is carried out using analytical models. The convective-diffusive heat flux at the stagnation point is computed using the Fay-Riddell [3] formula for

a totally catalytic wall, and is then distributed over the wall using the Vérant-Lefrançois model [4]. To model the material response, the ARES software includes the MoDeTheC code [5], which solves the 3D mass and heat transport equations in a porous medium and is based on a multi-component description for modelling internal degradation reactions. The wall temperature is determined by solving the following thermal balance:

$$\phi_{c+d}+\phi_{ab}=\phi_{cond}+\varepsilon\sigma_S\left(T_w^4-T_\infty^4\right) \quad (1)$$

where ϕ_{c+d} is the convective-diffusive heat flux, ϕ_{ab} the energy injected into the flow due to ablation and ϕ_{cond} the energy transmitted to the material by conduction (in $W.m^{-2}$). The last term is the radiative flux emitted by the wall (in $W.m^{-2}$).

Two different liners are considered (Aluminium and TiAl6V4) while the CFRP studied is the aerospace composite M55J/M18 [6]. In our simulations, the composite is described by 4 components (M18 matrix, M55J fibers, char, pyrolysis gas) whose relative composition evolves as a function of the advancement state of the following pyrolysis reaction:

$$Resin \rightarrow \nu\, Char+(1-\nu)Gas \quad (2)$$

with $\nu=0.21$, a reaction order $n=3.29$ and the reaction rate given by an Arrhenius law of parameters $A=5.1\times10^{13}s^{-1}$ and $E_A=2.03\times10^5 J.mol^{-1}$. Individual thermophysical properties of each component have been characterised and are homogenised using mixing laws to obtain equivalent properties of the composite during its degradation.

Simulations are initialised with atmospheric conditions at altitude $z=78\,km$, an entry velocity $V_\infty=7.7\,km/s$, an initial slope angle $\gamma=-0.1°$, and an angle of attack for the objects of $\alpha=0°$ or $90°$ (apart from the sphere). In total, 1484 different re-entry trajectories are calculated. The evolution of different quantities with respect to altitude is shown in Fig. 2. Since only the continuous regime is considered in this study, the curves are truncated when the Knudsen number Kn is greater than 10^{-3}.

This work being limited to the continuous hypersonic regime (M_∞>5), the study area boundaries are delineated by the red rectangle in Fig. 2a. The red dashed line represents the Space Shuttle trajectory [7]. This study therefore applies not only to space debris, but also to hypersonic vehicles re-entering the atmosphere from LEO. The convective-diffusive heat flux at the stagnation point reaches up to $1.8\,MW.m^{-2}$ (see Fig. 2b) corresponding to a wall temperature ranging between $450-2500K$ (see Fig. 2c). The maximum mass flux of pyrolysis gases at the stagnation point to be applied for CFD simulations to study the blowing effect is around $\dot{m}_{stag}=20\times10^{-3}kg.m^{-2}.s^{-1}$.

3. CFD simulations and pyrolysis gas blowing effects on wall heat flux

3.1. Setting up of the simulations

Three flight points were selected for the CFD simulations, at altitudes of 70, 60, and 50km and Mach numbers of 21, 15, and 9 respectively. These conditions are represented by the yellow dots in Fig. 2a. More details about the freestream conditions are provided in Table 1.

Simulations have been carried out using the CFD code CEDRE/CHARME developped at ONERA [8] on a 2D axisymmetric sphere of diameter $D=1\,m$, to assess the influence of pyrolysis products outgassing on the wall heat flux. The wall temperature is set constant along the surface between $T_w=1000-2500\,K$. Pyrolysis gases are blown at the wall on the front side of the object for $y/D\leq0.4$ at a temperature $T_{blow}=T_w$ and with a mass flux $\dot{m}_{stag}=0-20\times10^{-3}kg.m^{-2}.s^{-1}$. Two approaches are considered to assess the influence of outgassed species in the flow. On the one hand, blown pyrolysis gases are assumed to be chemically frozen, and a Park model [9] for the 5 species of dissociated air is used. On the other hand, both the air and outgassed species are in chemical non-equilibrium, and a kinetic model of 131 reactions derived from the work of Martin *et al.* [10] for the 28

neutral following species is used:

$$N_2, O_2, N, O, NO, C, C_2, C_3, C_2H, C_2H_2, CH, CH_2, CH_3, CH_4, CN, CO, CO_2,$$
$$H, H_2, H_2O, H_2O_2, HCN, HCO, HNO, HO_2, NCO, NH, OH$$

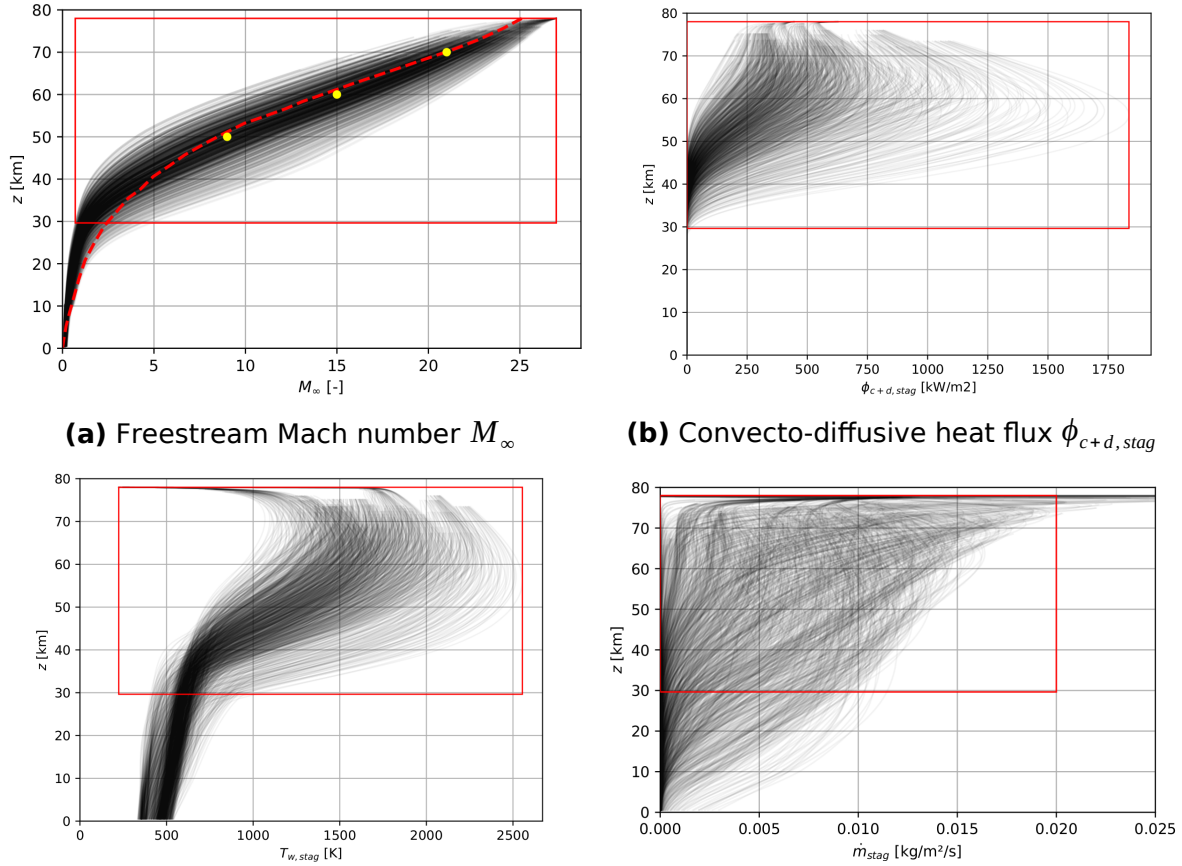

(a) Freestream Mach number M_∞

(b) Convecto-diffusive heat flux $\phi_{c+d,stag}$

(c) Wall temperature $T_{w,stag}$

(d) Pyrolysis gas mass blowing rate $\dot{m}_{stag}$

Fig 2. Evolution of Mach number and several quantities at stagnation point with respect to altitude z in the continuous regime for the simulated objects. The red rectangle delineates our domain of interest.

Table 1. Flight conditions for the CFD simulations.

N°	z [km]	M [−]	V_∞ [m · s^{-1}]	p_∞ [Pa]	T_∞ [K]
1	70	21	6238.14	5.22	219.58
2	60	15	4725.99	21.96	247.02
3	50	9	2968.12	79.78	270.65

The pyrolysis gas composition is taken from the work of Torres-Herrador *et al.* [11], who experimentally characterised the decomposition gases of an epoxy resin used in COPVs under different conditions. We have chosen the composition characterised during the Py600-R800 test, in which the material was degraded at a pyrolysis temperature of 600 °, and the decomposition gases analysed in a second reactor at 800 °. We believe that these conditions best represent the degradation of a CFRP during atmospheric re-entry, since the gases are first produced inside the material and then heat up as they are transported to the fluid-solid interface where they are finally ejected into the boundary layer. In their work, 70 species were identified, but we have only retained the species involved in Martin's reaction mechanism. The composition considered is a mixture of

$(H_2, H_2O, CO, CO_2, CH_4)$ with mass fractions of $(0.017, 0.283, 0.358, 0.093, 0.249)$ respectively. The flow is assumed to be in thermal equilibrium. The individual viscosities are obtained using a Blottner model and the conductivities are calculated using a Prandtl number specific to each species $Pr = 0.675 - 0.809$. A Wilke's mixing law is used to determine the mixture transport coefficients. The diffusion is modeled using a Fick's law with a global diffusivity computed for a constant Schmidt number $Sc = 0.864$ [12].

3.2. Influence of mass blowing rate and chemical non-equilibrium of pyrolysis gas on wall heat flux

Figure 3 shows the evolution of the dimensionless wall heat flux at stagnation point $(\phi/\phi_0)_{stag}$ with respect to the mass flux rate $\dot{m}$, at altitude $z = 70\,km$ and Mach number $M = 21$. The reference wall heat flux ϕ_0 is calculated without blowing $(\dot{m}_{stag} = 0\,kg.m^{-2}.s^{-1})$, hence $(\phi/\phi_0)_{stag}$ directly quantifies the blowing effects on wall heat flux modification.

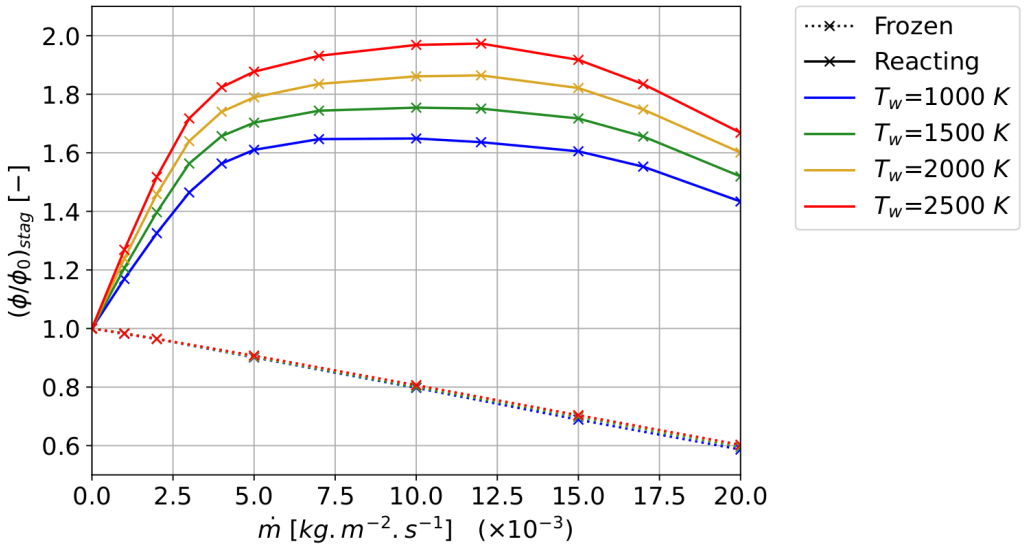

Fig 3. Influence of pyrolysis gas blowing on dimensionless wall heat flux for a 1 m diameter sphere at altitude $z = 70\,km$ and Mach number $M = 21$. Dotted and solid lines correspond to frozen and reacting blowing respectively. Coloured lines refer to different temperatures.

For chemically frozen pyrolysis gases (dotted lines) it is observed that the stronger the blowing rate, the lower the wall heat flux; which is well known as convective blocking. This linear trend is verified regardless of the wall temperature (*i.e.* blowing temperature) as the four curves are perfectly superimposed. To better understand the blowing effects on the near-wall flow, the evolution of the total chemical heat release rate $\dot{\omega}_T$ (in $J.m^{-3}.s^{-1}$) with respect to the wall distance d_w along the stagnation line is plotted in Fig. 4a for several blowing rates. This term is defined as:

$$\dot{\omega}_T = -\sum_{i=1}^{N_s} \dot{\omega}_i \Delta_f H_i^0 \tag{3}$$

where N_s is the number of species, $\dot{\omega}_i$ the molar production rate (in $mol.m^{-3}.s^{-1}$) and $\Delta_f H_i^0$ the formation enthalpy (in $J.mol^{-1}$). Figure 4a shows that blowing leads to a significant reduction of the energy generated close to the wall by exothermic reactions (mainly N_2 recombination reactions here), and shifts the reaction front upstream. In other words, these reactions occur earlier in the flow, which lowers the significance of exothermic reactions near the wall. Thus, the heat flux reduction results not only from the injection of cold gas reducing the temperature gradient in the boundary layer, but also from the attenuation of reactive effects close to the wall.

For outgassed species reacting with air, the new strongly exothermic reactions are responsible for an important increase of the wall heat flux compared to frozen blowing simulations, see Fig. 3 (solid lines). This results in much higher chemical heat release rate in the boundary layer, see Fig. 4b. For sufficiently low blowing mass flux $\left(\dot{m}_{stag} \leq 4 \times 10^{-3} kg.m^{-2}.s^{-1}\right)$, these reactions occur close enough to the wall and $\left(\phi/\phi_0\right)_{stag}$ increases linearly with respect to $\dot{m}$. For higher blowing rate $\left(\dot{m}_{stag} = 4 - 15 \times 10^{-3} kg.m^{-2}.s^{-1}\right)$, the wall heat flux is almost constant because of the competition between reactive and convective effects. Although more species are injected into the flow to react with the air and release energy, this phenomenon is counterbalanced by convective blocking becoming increasingly important. One can also note a peak for $\dot{\omega}_T$ in Fig. 4b, reflecting a localisation of the reactions moving upstream from the wall as $\dot{m}$ increases. At a sufficiently high blowing rate, reactions take place further away from the wall and the heat flux decreases as convective blocking prevails over reactive effects. Note that temperature has an effect on the intensity of this competition between reactive and convective regimes, but not on the qualitative behavior.

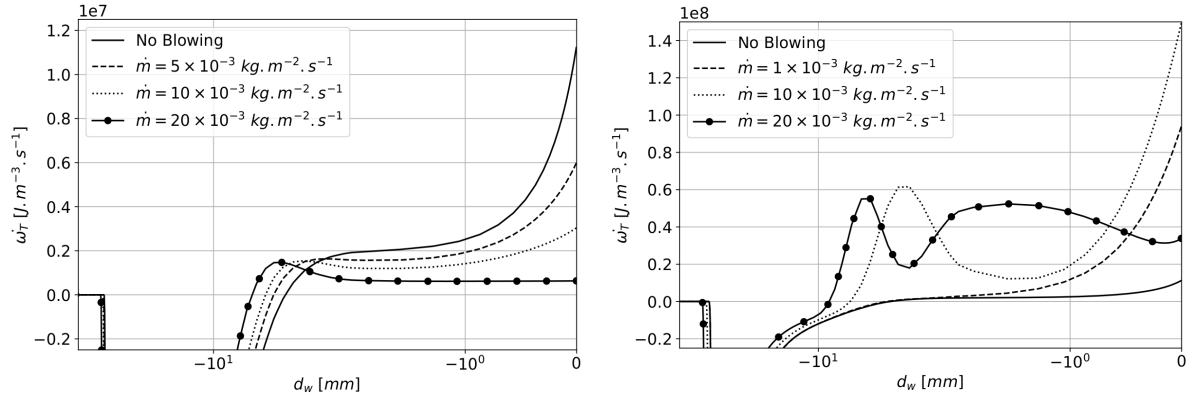

(a) Frozen pyrolysis gas. **(b)** Reacting pyrolysis gas.

Fig 4. Evolution of the total chemical heat release rate $\dot{\omega}_T$ with respect to the wall distance d_w along the stagnation line, for several mass blowing fluxes.

Figure 5 shows the results for flight conditions N°2 $\left(z = 60\,km, M = 15\right)$ and N°3 $\left(z = 50\,km, M = 9\right)$, see Table 1. Different chemical mecanisms are triggered between the three considered flight conditions, thus explaining the deviation on wall heat flux evolution. However, the general conclusions are identical, namely a linear decrease of the flux for frozen simulations, and a competition between exothermic reactions and convective blocking for reacting pyrolysis gases. The effect of temperature is unchanged.

3.3. Influence of the pyrolysis gas composition

Calculations have been carried out with different blowing gas mixtures to assess the influence of its composition on the evolution of heat flux. In addition to the Py600-R800 used so far, two compositions also taken from the work of Torres-Herrador *et al.* [11] are considered, namely Py400-R350 and Py600-R350. The resin was first degraded at a pyrolysis temperature of $400\,°$, respectively $600\,°$, and the decomposition gases characterised in a second reactor at $350\,°$. Two binary mixtures of CO/CO_2 and H_2/H_2O are also investigated. These five compositions are summarised in Table 2. Finally, simulations are also conducted with pure blowing composition, for each of the five following species: $H_2, H_2O, CO, CO_2, CH_4$. Figure 6 compares the evolution of $\left(\phi/\phi_0\right)_{stag}$ with respect to $\dot{m}$ for the ten blowing compositions considered, for a 1 m diameter sphere with flight conditions N°1, see Table 1.

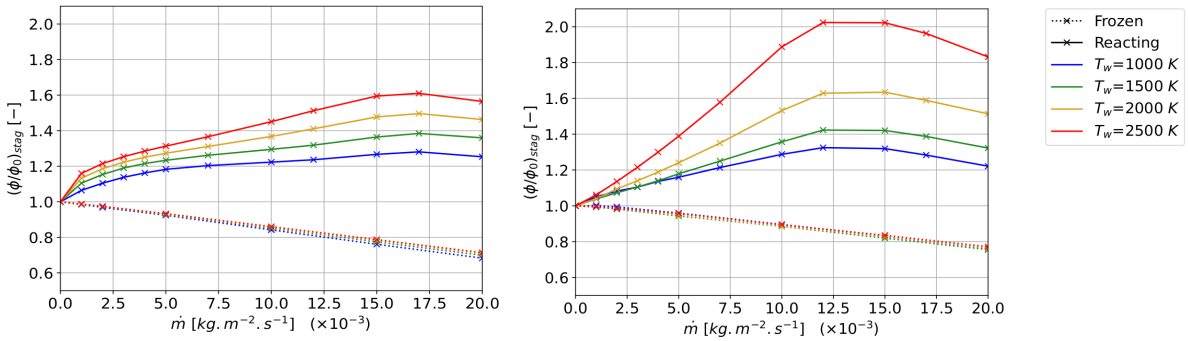

(a) $z=60\,km$, $M=15$. **(b)** $z=50\,km$, $M=9$.

Fig 5. Influence of pyrolysis gas blowing on dimensionless wall heat flux for a 1 m diameter sphere for different flight conditions. Dotted and solid lines correspond to frozen and reacting blowing respectively. Coloured lines refer to different temperatures.

Table 2. Mixtures considered as pyrolysis gas, expressed in mass fraction.

Name	H_2	H_2O	CO	CO_2	CH_4
Py600-R800	0.017	0.283	0.358	0.093	0.249
Py400-R350	0.	0.793	0.030	0.162	0.015
Py600-R350	0.	0.468	0.122	0.355	0.055
CO/CO_2	0	0	0.794	0.206	0
H_2/H_2O	0.057	0.943	0	0	0

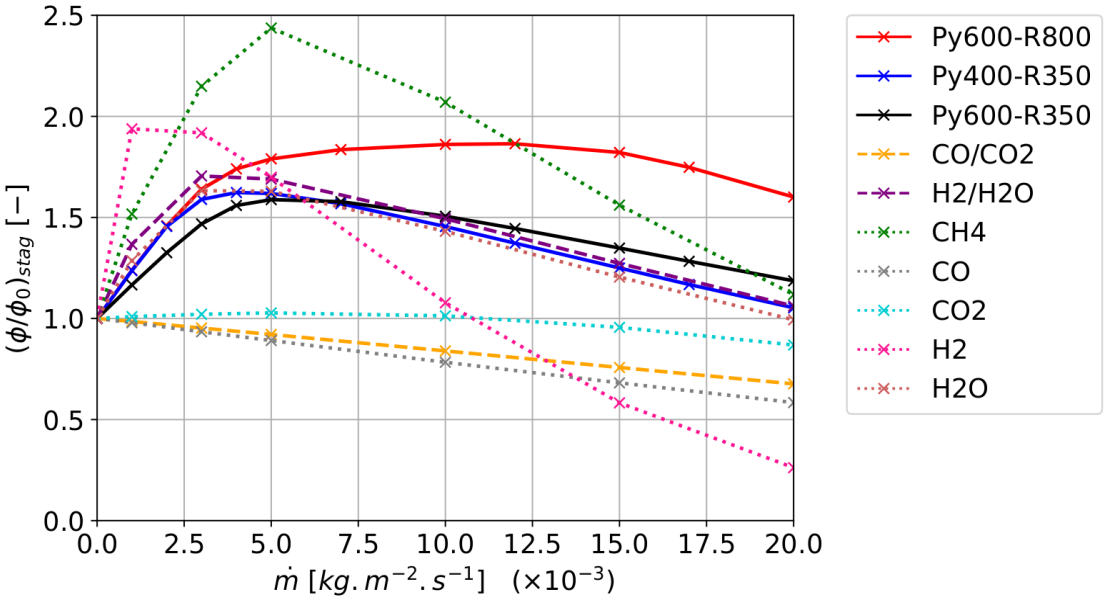

Fig 6. Influence of outgassed species composition on dimensionless wall heat flux for a 1m diameter sphere at altitude $z=70\,km$ and Mach number $M=21$.

There are significant differences in the heat transfer evolution between the compositions. Competition reactive and convective regimes is observed for all three experimental compositions (Py600-R800, Py400-R350, Py600-R350), for the binary mixture H_2/H_2O, as well as for the pure species H_2, H_2O, and CH_4. These three species interact with air in highly exothermic reactions close to the wall, increasing heat transfer, as previously described. By contrast, the influence of reactions between CO/CO_2 and air appears to be

too small to cause an increase in wall heat flux. Under boundary layer temperature and pressure conditions, the non-equilibrium between the two species favors CO. However, the dissociation reactions $CO_2+M \rightarrow CO+O+M$ and $CO_2+O \rightarrow CO+O_2$ are endothermic, with standard enthalpy of reaction $\Delta_r H^0 = 540\,kJ.mol^{-1}$ and $\Delta_r H^0 = 40\,kJ.mol^{-1}$ respectively. This may explain why convective effects prevail even at low blowing rates. This significant difference between CO/CO_2 and $H_2/H_2O/CH_4$ seems to show that H-derived components are strong catalysts for reactions with air in the boundary layer. Competition between reactive and convective regimes is thus to be expected when such species are degassed.

4. Discussion on the influence of mixture transport properties modelling fidelity

For atmospheric re-entry simulations, it is common practice to determine the individual species viscosity thanks to Blottner's curve fits, and thermal conductivities using Eucken or Prandtl's relation. The transport coefficients of the multi-component mixture can then be obtained with a Wilke's mixing rule. The effective diffusion coefficient is usually obtained by considering a constant Lewis or Schmidt number for all species. However, Alkandry *et al.* [13,14] showed a deviation of $15-60\%$ on the wall heat flux at the stagnation point of the Stardust reentry capsule (reentry velocity $V_\infty = 12.6\,km.s^{-1}$), between this regular modelling strategy and a higher fidelity modelling using Gupta-Yos' mixing rule and collision cross-section data to compute individual transport properties. In their work, nitrogen catalytic recombination and surface bulk oxydation was accounted for using the Driver *et al.* [15,16] model, but pyrolysis gas effects were neglected. Here, we intend to evaluate the difference between a high-fidelity and a Wilke/Blottner/Prandtl model with constant Schmidt number for LEO re-entry conditions ($V_\infty = 7.8\,km.s^{-1}$), in the presence of a pyrolysis gas blowing. High-fidelity simulations are conducted using the fortran library EGLIB [17], enabling multi-component transport coefficients to be calculated by solving the linear transport systems for viscosity, and for thermodiffusion including Soret and Dufour effects. The thermodynamic data needed to calculate the matrix terms are taken from [18]. A comparison of the wall heat flux evolution is shown for frozen and reacting blowing for the three flight conditions in Fig. 7.

Overall, the Wilke/Blottner/Prandtl modelling strategy are in good aggreement with EGLIB. Regardless of freestream conditions, the two models match perfectly without blowing ($\dot{m} = 0\,kg.m^{-2}.s^{-1}$) and for frozen outgassed species. However for reacting simulations, the Wilke model overestimates the heat transfer compared to EGLIB simulations. This deviation progressively widens as the mass blowing rate increases, up to 20% for the freestream conditions at altitude $z = 70\,km$, 10% at altitude $z = 60\,km$, and 5% for the last flight conditions at altitude $z = 50\,km$. These differences are attributed to several causes. Firstly, modelling the diffusion coefficients with constant Schmidt obviously gives different results from EGLIB. The composition in the boundary layer varies from one model to another, even slightly, and leads to different reaction paths and chemical heat release rates. The individual species properties depend directly on temperature via the Blottner and Prandtl models, so conductivity varies greatly close to the wall. In addition, Wilke's mixing law depends directly on each species' molar fraction. Finally, a deviation in the estimated composition and individual transport properties naturally leads to a variation in the heat flux at the wall. This discrepancy increases for reactive blowing and with the blowing rate, as more species are injected and react with the air, thus increasing the differences in the reaction paths adopted between the two models. As temperature decreases, *i.e.* for a weaker shock upstream of the object, the level of air dissociation in the boundary layer is lower and reactions with outgassed species are less significant. This may explain the reduced differences between Wilke/Blottner/Prandtl with constant Schmidt, and EGLIB for flight points at lower altitudes and Mach numbers.

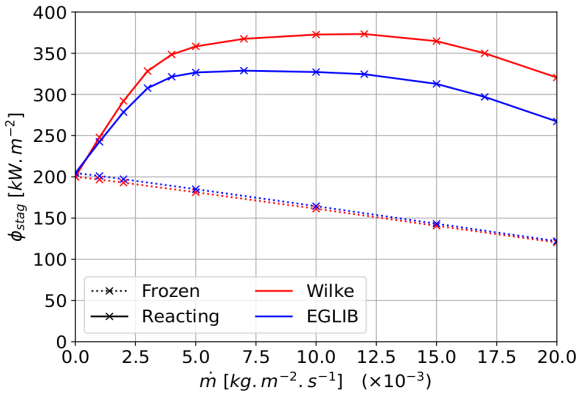

(a) $z = 70\,km$, $M = 21$.

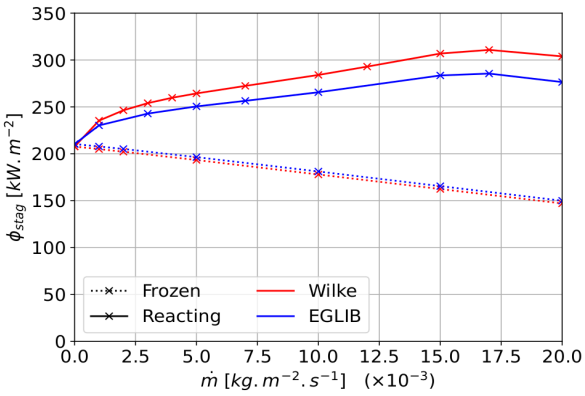

(b) $z = 60\,km$, $M = 15$.

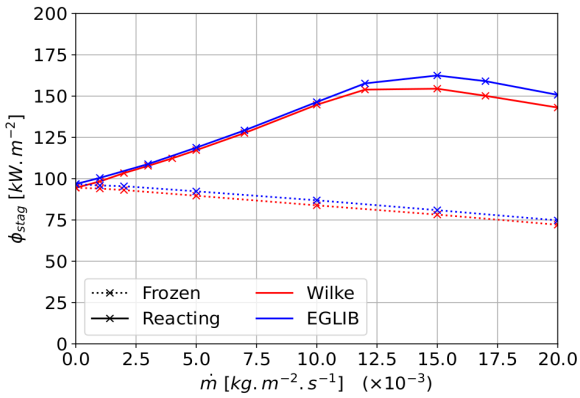

(c) $z = 50\,km$, $M = 9$

Fig 7. Influence of mixture transport properties modelling on wall heat flux for a 1 m sphere for several flight conditions. Dotted and solid lines correspond to frozen blowing, respectively reacting. Coloured lines refer to different transport properties models.

5. Conclusions and perspectives

The goal of this work was to study the influence of pyrolysis gas blowing on wall heat flux modification for charring materials. Firstly, 1484 re-entry trajectories were calculated on different simple geometries. This made it possible to define the study domain in terms of wall heat flux, temperature, and mass blowing rate at the wall, and then to extract characteristic flight points on which to carry out CFD simulations. The influence of the blowing rate, the temperature, and the reactions between the degassed species and the air were studied for a 1m diameter sphere and three freestream conditions. For a frozen blowing, the heat flux decreases linearly and independently of the temperature. For a reacting blowing, there is a reactive regime preceding a convective regime, as a result of competition between exothermic reactions taking place close to the wall and convective effects injecting a cold gas and shifting the reactions upstream. Secondly, the influence of the ejected gas composition was studied for conditions corresponding to an altitude of $z = 70\,km$ and a Mach number of 21. Under these specific conditions, significant differences were observed. In particular, a blowing composed exclusively of CO/CO_2 does not lead to an over-increase in the heat transfer because these species react very little with the air. On the contrary, it seems that the H-derived species have a strong reaction potential with air. Finally, the classical Wilke/Blottner/Prandtl modelling strategy with constant Schmidt was compared with high-fidelity modelling based on the EGLIB library. Without blowing or for a frozen blowing, both models predicted the same levels of heat flux. However, a difference of up to 20% is observed for reactive outgassing, as the blowing and the enthalpy conditions of the flow increase. This difference is probably due to

the diffusivity being modelled using a constant Schmidt number. Small variations of the boundary-layer composition have major consequences on temperature, individual species transport properties, the determination of the mixing properties and, finally, the wall heat flux.

This work is a first milestone in providing an overview of the influence of the phenomena associated with the degradation of charring materials on wall heat flux modification. A study of the effects of physico-chemical wall processes (catalytic recombination, oxidation, nitridation, sublimation) should then be carried out. This will make it possible to define the input parameters for the learning base generation, on which supervised machine learning techniques will be applied.

Acknowledgements

This work was supported by the ONERA and ”Centre National d’Études Spatiales” (French Space Agency) through the co-funding of the Ph.D. of M. Lalande.

References

1. Prévereaud, Y.: Contribution à la Modélisation de la Rentrée Atmosphérique des Débris Spatiaux (Development of Models for the Atmospheric Re-Entry of Space Debris), Ph.D. thesis, Université de Toulouse, France (2014). https://hal.archives-ouvertes.fr/tel-01171757/file/DMAE15028.1434445612.pdf
2. Lips, T., Fritsche, B., Kanzler, R., Schleutker, T., Gülhan, A., Bonvoisin, B., Soares, T., Sinnema, G.: About the Demisability of Propellant Tanks During Atmospheric Re-Entry From LEO. Journal of Space Safety Engineering, 4(2):99–104 (2017). https://doi.org/10.1016/j.jsse.2017.07.004
3. Fay, J., Riddell, F.: Theory of Stagnation Point Heat Transfer in Dissociated Air, Journal of the Aerospace Sciences 73–85 (1958). https://doi.org/10.2514/8.7517
4. Prévereaud, Y., Vérant, J.-L., Balat-Pichelin, M., Moschetta, J.-M.: Numerical and Experimental Study of the Thermal Degradation Process During the Atmospheric Re-Entry of a TiAl6V4 Tank, Acta Astronautica 122 258–286 (2016). https://doi.org/10.1016/j.actaastro.2016.02.009
5. Dellinger, N., Leplat, G., Huchette, C., Biasi, V., Feyel, F.: Numerical Modeling and Experimental Validation of Heat and Mass Transfer Within decomposing Carbon Fibers/Epoxy Resin Composite Laminates, International Journal of Thermal Sciences (2024).
6. Perron, N.: Modélisation de la Dégradation Thermo-Structurale des Débris Spatiaux durant la Rentrée Atmosphérique (Thermo-Structural Decomposition Modelling of Space Debris during Atmospheric Entry). Ph.D. thesis, Université de Toulouse, France (2022). https://depozit.isae.fr/theses/2022/2022_Perron_Nicolas_D.pdf
7. Anderson, J.: Hypersonic and High Temperature Gas Dynamics, AIAA (1989).
8. Refloch, A., Courbet, B., Murrone, A., Villedieu, P., Laurent, C., Gilbank, P., Troyes, J., Tessé, L., Chaineray, G., Dargaud, J.B., et al.: CEDRE Software. Aerospace Lab, (2) (2011).
9. Park, C.: Review of Chemical-Kinetic Problems of Future NASA Missions, I: Earth Entries, Journal of Thermophysics and Heat transfer 7 (3) 385–398 (1993). https://doi.org/10.2514/3.431
10. Martin, A., Cozmuta, I., Wright, M.J., Boyd, I.D.: Kinetic Rates for Gas-Phase Chemistry of Phenolic-Based Carbon Ablator in Atmospheric Air, Journal of Thermophysics and Heat Transfer 29 (2) 222–240 (2015). https://doi.org/10.2514/1.T4184
11. Torres-Herrador, F., Eschenbacher, A., Blondeau, J., Magin, T.E., Van Geem, K.M.: Study of the Degradation of Epoxy Resins Used in Spacecraft Components by

Thermogravimetry and Fast Pyrolysis. Journal of Analytical and Applied Pyrolysis, 161:105397 (2022). https://doi.org/10.1016/j.jaap.2021.105397

12. William, J.: Étude des Processus Physico-Chimiques dans les Écoulements Détendus à Haute Enthalpie: Application à la Soufflerie à Arc F4 (Study of Physico-Chemical Processes in High Enthalpy Expanded Flows: Application to the F4 Hot-Shot Wind Tunnel). Ph.D. thesis, Aix-Marseille 1 (1999)
13. Alkandry, H., Boyd, I.D., Martin, A.: Comparison of Models for Mixture Transport Properties for Numerical Simulations of Ablative Heat-Shields. In 51st AIAA Aerospace Sciences Meeting including the New Horizons Forum and Aerospace Exposition, page 303 (2013). https://doi.org/10.2514/6.2013-303
14. Alkandry, H., Boyd, I.D., Martin, A.: Comparison of Transport Properties Models for Flowfield Simulations of Ablative Heat Shields. Journal of Thermophysics and Heat Transfer, 28(4):569–582 (2014) https://doi.org/10.2514/1.T4233
15. Driver, D., Olson, M., Barnhardt, M., MacLean, M.: Understanding High Recession Rates of Carbon Ablators Seen in Shear Tests in an Arc Jet. In 48th AIAA Aerospace Sciences Meeting Including the New Horizons Forum and Aerospace Exposition, page 1177 (2010). https://doi.org/10.2514/6.2010-1177
16. Driver, D., MacLean, M.: Improved Predictions of PICA Recession in Arc Jet Shear Tests. In 49th AIAA Aerospace Sciences Meeting Including the New Horizons Forum and Aerospace Exposition, page 141 (2011). https://doi.org/10.2514/6.2011-141
17. Ern, A., Giovangigli, V.: Fast and Accurate Multicomponent Transport Property Evaluation. Journal of Computational Physics, 120(1):105–116 (1995). https://doi.org/10.1006/jcph.1995.1151
18. Kee, R.J., Rupley, F.M., Miller, J.A., Coltrin, M.E., Grcar, J.F., Meeks, E., Moffat, H.K., Lutz, A.E., Dixon-Lewis, G., Smooke, M.D., et al.: CHEMKIN Collection, Release 3.6, Reaction Design. Inc., San Diego, CA, 20 (2000).